Cocaine disinhibits dopamine neurons by potentiation of GABA transmission in the ventral tegmental area

Bocklisch, Christina; Pascoli, Vincent Jean; Wong, Jovi Chau-Yee; House, David; Yvon, Cédric Marcel; De Roo, Mathias; Luescher, Christian; Tan, Kelly

How to cite

BOCKLISCH, Christina et al. Cocaine disinhibits dopamine neurons by potentiation of GABA transmission in the ventral tegmental area. In: Science, 2013, vol. 341, n° 6153, p. 1521–1525. doi: 10.1126/science.1237059

This publication URL: https://archive-ouverte.unige.ch/unige:33842

Publication DOI: 10.1126/science.1237059

Cocaine disinhibits dopamine neurons by potentiation of GABA transmission in the VTA

Authors: Christina Bocklisch[1], Vincent Pascoli[1], Jovi C. Wong[1]†, David R.C. House[1], Cédric Yvon[1], Mathias de Roo[1], Kelly R. Tan[1], and Christian Lüscher[1,2]

Affiliations:

[1] Dept. of Basic Neurosciences, Medical Faculty, University of Geneva, CH-1211 Geneva, Switzerland.

[2] Clinic of Neurology, Dept. of Clinical Neurosciences, Geneva University Hospital, CH-1211 Geneva, Switzerland.

* Correspondence to: christian.luscher@unige.ch

† Current address: Nuffield Laboratory of Ophthalmology, Nuffield Department of Clinical Neurosciences, University of Oxford, UK

Abstract: Drug-evoked synaptic plasticity in the mesolimbic system reshapes circuit function and eventually leads to compulsive behavior, which defines addiction. Much research has focused on excitatory transmission in the ventral tegmental area (VTA) and the nucleus accumbens (NAc) where several forms of adaptive synaptic plasticity have been characterized. How drug-evoked synaptic plasticity of inhibitory transmission shapes circuit adaptations remains unknown. Here we demonstrate that the medium spiny neurons (MSNs) expressing dopamine (DA) receptor type 1 (D1R-MSNs) of the NAc project to the VTA with a strong preference for GABA neurons. We observe that chronic *in vivo* exposure to cocaine evokes synaptic potentiation at this synapse, which occludes homosynaptic inhibitory long-term potentiation (iLTP). As a consequence the activity of the VTA GABA neurons is reduced and DA neurons are disinhibited, facilitating the development of locomotor sensitization. Cocaine-evoked potentiation of GABA release from D1R-MSNs of the NAc is therefore permissive for drug-adaptive behavior, which identifies these neurons as a promising target for novel addiction treatments.

One Sentence Summary: Cocaine-evoked potentiation of the inhibitory transmission onto VTA GABA neurons chronically disinhibits DA neurons and facilitates drug-adaptive behavior. (149 char).

Main Text: Disinhibition, that is the removal of an inhibitory break on neuronal firing, may affect circuit function in several part of the brain (*1-3*). For example, disinhibition of VTA DA neurons has been implicated in drug reinforcement when, in the acute phase, the addictive drug shuts down VTA GABA neurons (e.g. opioids (*4*), benzodiazepines (*5*), and gamma hydroxybutyrate (*6*)). To understand how this monosynaptic building block integrates into the larger circuitry, we characterized the functional anatomy of the inhibitory projections to the VTA. We focused on the major input that originates in the NAc. As in the dorsal striatum, accumbal MSNs fall into two classes, the D1R-MSNs and D2R-MSNs (*7*), which may segregate with the projection target. To reveal the type of MSN projecting to the midbrain, we injected a retrograde tracer (B subunit of cholera toxin) fused to a fluorescent cyanine dye (CTB-Cy3) into the VTA of BAC transgenic mice where the expression of enhanced green fluorescent protein (EGFP) is driven by the promotors of D1- or D2-receptors respectively (D1R-EGFP and D2R-EGFP mice, Fig. 1A). We then counted the CTB-Cy3 positive cells and determined the co-localization with EGFP in neurons of the NAc of both mouse lines (Fig. 1B, Hoechst, a nuclear staining, was used to obtain the total number of cells, n = 1721 and 1922 in D1R-EGFP and D2R-EGFP mice, 3 animals each). EGFP positive cells accounted for about half of all cells (D1R-mice: 52 ± 2 %, D2R-EGFP mice: 43 ± 1 %, Fig. 1C). A smaller fraction of cells, similar in both mouse lines, was positive for CTB-Cy3 (D1R-EGFP mice: 34 ± 8 %, D2R-EGFP mice: 33 ± 4 %, Fig. 1C). Co-localization with EGFP was observed only in D1R-EGFP mice (Fig. 1B, C). Hence, only D1R-MSNs project directly to the midbrain, akin to the dorsal striatum.

Since the VTA contains GABA and DA neurons (*8*) and recent studies have suggested that MSNs of the NAc project to both (*9, 10*), we aimed to characterize the functional connectivity between MSNs and VTA neurons. We expressed ChR2 in the NAc of mice that expressed a fluorescent marker in VTA GABA neurons (GAD65-tdTomato) and prepared acute slices of the VTA (Fig. 1D). We recorded from both, tdTomato-positive and -negative neurons (Fig. 1E) and induced GABA release by wide-field illumination. Large inhibitory postsynaptic currents (IPSCs) were elicited in the majority (87.4 %) of tdTomato-positive neurons (497 ± 89 pA, n = 17), while only a small fraction of tdTomato-negative neurons was responsive (8.33 %, 20.3 ± 15.2 pA, n = 24, Fig. 1F). Both picrotoxine (PTX 100 μM, n = 3) and tetrodotoxin (TTX 0.5 μM,

n = 4, not shown) abolished the IPSCs in td-Tomato-positive neurons, confirming action potential dependent transmitter release followed by $GABA_A$ receptor activation (Fig. 1E). Clearly, accumbal MSNs exert strong inhibiton onto VTA GABA neurons. In order to reveal a possible functionally weaker connectivity onto DA neurons due to technical threshold, we expressed the more efficient ChR2(H134R) (*11*) into the NAc of Pitx3-GFP mice (a marker for DA neurons, (*12*)). Under these circumstances, we were able to detect small IPSCs in 67% of the Pitx3-GFP-positive cells (127 ± 44 pA, n = 12) and large IPSCs in 100% of GFP negative neurons (1602 ± 473 pA, n =10, Fig. 1G, H). Thus, although a direct inhibitory projection onto VTA DA neurons exists (*10*), we found a much more frequent and stronger inhibitory connection onto VTA GABA cells, in line with a previous study (*9*). Given the strong evidence for the inhibition of DA neuron firing by local GABAergic cells (*13*) this suggested that D1R-MSNs of the NAc could drive disinhibition of VTA DA neurons.

To test this possibility, we performed *in vivo* single unit recordings of VTA neurons in response to optical stimulation of MSN terminals in the VTA in anaesthetized mice (Fig. 1I). We first recorded from GABA neurons, confirmed by juxtacellular labelling methods and post hoc immunohistochemistry (Fig. 1J, top). As predicted, all GABA neurons responded to a 2 s light pulse with decreased spiking activity (-92.2 ± 2 % of baseline activity, n = 4, Fig. 1K). We next recorded from DA neurons (Fig. 1J, bottom, L), whose activity was increased when the blue light was flashed (146.8 ± 10.5 % of baseline, n = 7, $p < 0.05$). Thus, despite a weak direct inhibitory connection to VTA DA neurons, D1R-MSN terminal activation leads to their disinhibition. This scenario was confirmed when we expressed the inhibitory opsin effector halorhodopsin (eNpHR3.0) selectively in VTA GABA neurons as an increase in DA neuron activity during a 2 s amber light activation was observed (Supplementary Fig. S1). We conclude that NAc D1R-MSNs suppress the tonic activity of VTA GABA neurons, which disinhibits VTA DA neurons.

With the addictive drugs listed above, it is generally assumed that disinhibition is fully reversed once the drugs are eliminated. Here we posit the hypothesis that the disinhibitory circuit in the VTA may undergo persistent remodelling with chronic drug exposure. We therefore wanted to know whether the synapse between D1-MSNs and VTA GABA neurons is capable of expressing activity-dependent synaptic plasticity. We elicited GABA release from axonal terminals in the

VTA with blue light and recorded from VTA GABA neurons (Fig. 2A). High-frequency stimulation (HFS, Fig. 2A) of MSN terminals led to a robust potentiation of light-evoked IPSCs (183 ± 22 % of baseline, n = 15, $p < 0.05$, Fig. 2B). This iLTP, which could also be induced with low Cl^--containing internal solution (135 ± 8 % of baseline, n = 8, $p < 0.01$, Supplementary Fig. S2A), was associated with a decrease of the failure rate (baseline: 0.29 ± 0.07, after HFS: 0.2 ± 0.06, n = 12, $p < 0.01$), changed variance ($1/CV^2$, baseline: 2.02 ± 0.54, after HFS: 4.23 ± 1.26, n = 15, $p < 0.01$) while the reduction of the paired pulse ratio (PPR) was not significant due to a high variance (baseline: 1.02 ± 0.19, after HFS: 0.93 ± 0.08, n = 15, $p > 0.05$, Fig. 2C). The three parameters in combination strongly suggest an increase in release probability. In line with this interpretation, infusion of a high concentration of the calcium chelator BAPTA (10 mM) into the postsynaptic neuron did not block iLTP (160 ± 20 % of baseline, n = 14, $p < 0.01$, Fig. 2D) while the calcium channel blocker nimodipine applied extracellularly (Nim, 10 µM) abolished the potentiation (91 ± 18 % of baseline, n = 7, $p > 0.05$, Fig. 2E). Presynaptic forms of synaptic plasticity have been shown to depend on the cAMP-PKA cascade (*14*), hence we aimed to stimulate potentiation with the adenylyl cyclase (AC) activator forskolin (FSK, 10 µM). This caused a potentiation of the transmission (178 ± 32 % of baseline, n = 11, $p < 0.01$, Fig 2F, black trace), which occluded the ability of HFS to induce iLTP (86 ± 6 % of baseline, n = 4, $p > 0.05$, Fig. 2F, grey trace). The underlying mechanism therefore likely involves this cascade in the terminals of NAc MSNs. We confirmed that FSK-induced potentiation is solely mediated by presynaptic PKA by additionally loading the postsynaptic cell with the membrane-impermeable PKA inhibitor PKI 6-22 (20 µM) while bath applying FSK (Supplementary Fig. S2B). Taken together, induction as well as expression of iLTP is likely to be presynaptic, akin to well-described forms of potentiation at hippocampus mossy fiber excitatory synapses (*15*). Since this "sister" LTP requires the scaffolding protein Rim1α (*16*), we tested its involvement in iLTP and found that HFS in the $Rim1\alpha^{-/-}$ mice left basal IPSC amplitudes unaffected (97 ± 14 % of baseline, n = 7, $p > 0.05$, Fig. 2G). Hence, iLTP in the VTA also depends on presynaptic Rim1α.

With the characterization of the functional anatomy at hand, we wanted to next test whether inhibitory transmission between D1R-MSNs and VTA GABA neurons was affected by chronic drug exposure. We chose cocaine not only because it is a highly addictive drug that evokes synaptic plasticity at several excitatory synapses of the mesolimbic system (*17*), but also because

its reinforcing effects are mediated by directly increasing DA concentration in the NAc instead of disinhibiting DA neurons (cocaine actually briefly *inhibits* DA firing in the acute phase, (*18*)). To test for cocaine-induced synaptic plasticity at this disinhibitory circuit, we chronically treated mice with cocaine (15mg/kg i.p. for 5 days, Fig. 3A), prepared midbrain slices 24h after the last injection and examined whether this treatment interfered with the ability to elicit iLTP. We found that the drug exposure disrupted HFS-induced iLTP (saline: 157 ± 29 % of baseline, n = 9; cocaine: 86 ± 7 % of baseline, n = 9, $p < 0.05$ Fig. 3B) and was associated with a decrease of the paired pulse ratio (saline: 1.28 ± 0.09, n = 27; cocaine: 0.82 ± 0.09, n = 19, $p < 0.01$, Fig. 3C) indicating an occlusion scenario. Moreover, bath-application of FSK readily potentiated light-evoked IPSCs in slices from saline treated animals, whereas it failed to potentiate the IPSCs in the cocaine group (saline: 249 ± 51 % of baseline, n = 9; cocaine: 101 ± 15 % of baseline, n = 8, $p < 0.05$, Fig. 3D), confirming the involvement of cAMP-PKA cascade in the induction of cocaine-evoked synaptic plasticity.

We next wanted to test whether induction of cocaine-evoked inhibitory plasticity was dependent on the increase of extracellular DA concentration (and not mediated via serotonin or noradrenalin transporter inhibition). We therefore exposed mice carrying a mutated cocaine insensitive DAT (DAT_{KI}, (*19*)) chronically to cocaine. In DAT_{KI} mice, cocaine treatment didn't disrupt the *ex vivo* iLTP (223 ± 38 % of baseline, n = 12, $p < 0.05$) while potentiation was not fully induced in heterozygous littermates (126 ± 23 % of baseline, n = 7, $p < 0.05$, Fig. 3E). This indicates that without DAT inhibition cocaine does not disrupt iLTP and thus confirms that *in vivo* cocaine-evoked synaptic plasticity on the other hand is induced by a dopamine-dependent mechanism.

The decreased PPR values suggest an enhanced GABA release probability at D1R-MSN terminals after cocaine treatment. To confirm this interpretation, we recorded spontaneous inhibitory synaptic currents (sIPSCs) after chronic cocaine treatment (Fig. 3F, G, H). Cocaine increased the sIPSC frequency in GABA neurons (saline: 7.05 ± 1.05 Hz, n = 11; cocaine: 16.23 ± 4.11 Hz, n = 12, $p < 0.05$, with a trailing enhancement of the amplitudes: saline: 55.97 ± 5.1 pA, n = 11; cocaine 72.64 ± 10.95 pA, n = 12, $p > 0.05$, Fig. 3F, G) but not in DA neurons, where the frequency of sIPSC was in fact lower in slices from cocaine treated mice (frequencies: saline: 14.73 ± 2.46 Hz, n = 11; cocaine: 7.35 ± 1.43 Hz, n = 10, $p < 0.05$, amplitudes: saline: 47.14 ± 3.28 pA, n = 11; cocaine 40.47 ± 2.1 pA, n = 10, Fig. 3F, H), in line with a depressed

inhibition reported previously (*20*, *21*). Taken together our data suggest a chronic disinhibition of VTA DA neurons, most likely through the potentiation of inhibitory synaptic transmission onto GABA neurons through a presynaptic mechanism. If this is the case, then the basal firing activity of VTA DA neurons should be increased after chronic cocaine treatment. Indeed, DA neurons showed increased spiking activity after chronic cocaine treatment compared to saline injected mice (saline: 3.4 ± 0.6 Hz, n = 23; cocaine: 9.0 ± 1.7 Hz, n = 16, $p < 0.01$, Fig. 3I) whereas GABA neurons fired at lower rates after cocaine (saline: 9.9 ± 2.1 Hz, n = 20; cocaine: 5.1 ± 1 Hz, n = 15, $p < 0.05$, Fig. 3I). Elevated firing activity of DA neurons is unlikely to result from increased direct excitation onto these cells, as one single injection of cocaine, which is known to increase glutamatergic tone onto DA neurons (*22*), failed to increase firing rates of DA neurons 24 h after the injection (Supplementary Fig. S3). Taken together cocaine selectively potentiates GABA release from NAc D1R-MSN terminals in a DA dependent fashion such that VTA DA neurons, are tonically disinhibited on the long run.

What might be the consequence for drug adaptive behavior? We opted to test for locomotor sensitization, a model for incentive saliency of cocaine that is observed after five daily injections, just as cocaine-evoked inhibitory plasticity (*23*). We applied the iLTP induction protocol *in vivo* and quantified the locomotor behaviour in response to cocaine injections on subsequent days (Fig. 4A, B, C). We found that one session of HFS in ChR2-AAV infected animals was sufficient to induce enhanced locomotor sensitization to cocaine, as compared to animals injected with a control AAV (15 minutes that follow the fifth cocaine injection, ctrl AAV: 666 ± 82 ¼ turns/15 min, n = 15; ChR2 AAV: 1243 ± 155 ¼ turns/15 min, n = 11, $p < 0.01$, Fig. 4D).

Discussion

We show that activity- and drug- induced plasticity in a disinhibitory circuit between D1R-MSNs and VTA GABA neurons shapes drug-adaptive behavior, here locomotor sensitization. The cellular correlate of the disinhibition is a form of homosynaptic potentiation of GABA transmission onto VTA GABA neurons. This cocaine-evoked inhibitory plasticity is DA-dependent and expressed presynaptically. As a consequence VTA DA neurons fire at higher frequencies, which facilitates the induction of locomotor sensitization. This adaptation of the inhibitory limb of the mesolimbic circuitry occurs in parallel with a strengthening of excitatory

afferents onto DA neurons in the VTA (*22*, *24*, *25*). After several days of withdrawal, excitatory transmission in the NAc then also adapts. Given the spiralling connectivity between VTA and NAc (*26*), drug-evoked synaptic plasticity in back-projecting D1R-MSNs emerges as a crucial step in circuit remodelling (*27*). It is of interest to note that D1R-MSNs undergo presynaptic and postsynaptic changes (*28*), resulting in an overall strengthening of its inhibitory effects. This may eventually drive alterations in the extended mesolimbic circuit, leading to additional behavioral adaptations such as cue-induced cocaine seeking or incubation of craving (*29, 30*). Clearly a picture is emerging of mesolimbic circuit remodelling that affects excitatory as well as inhibitory transmission with the effect to enhance D1R-MSN function. Controlling the activity of the D1R-MSNs, with pharmacological means or neuromodulation may therefore emerges as an appealing target for novel therapeutic interventions in addiction.

References and Notes:

1. J. J. Letzkus *et al.*, *Nature* **480**, 331 (2011).

2. F. Gambino, A. Holtmaat, *Neuron* **75**, 490 (2012).

3. R. C. Froemke, M. M. Merzenich, C. E. Schreiner, *Nature* **450**, 425 (2007).

4. S. W. Johnson, R. A. North, *J Neurosci* **12**, 483 (1992).

5. K. R. Tan *et al., Nature* **463**, 769 (2010).

6. H. G. Cruz *et al.*, *Nat Neurosci* **7**, 153 (2004).

7. J. Bertran-Gonzalez *et al., Journal of Neurosci* **28**, 5671 (2008).

8. S. R. Sesack, A. A. Grace, *Neuropsychopharmacology* **35**, 27 (2010).

9. Y. Xia *et al., J Neurosci* **31**, 7811 (2011).

10. M. Watabe-Uchida, L. Zhu, S. K. Ogawa, A. Vamanrao, N. Uchida, *Neuron* **74**, 858 (2012).

11. G. Nagel *et al.*, *Current Biology* **15**, 2279 (2005).

12. M. P. Smidt *et al.*, *Proc Natl Acad Sci USA* **94**, 13305 (1997).

13. K. R. Tan *et al., Neuron* **73**, 1173 (2012).

14. M. G. Weisskopf, P. E. Castillo, R. A. Zalutsky, R. A. Nicoll, *Science* **265**, 1878 (1994).

15. P. E. Castillo, *Cold Spring Harb Perspect Biol* **4** (2012), doi:10.1101/cshperspect.a005728.

16. P. E. Castillo, S. Schoch, F. Schmitz, T. C. Südhof, R. C. Malenka, *Nature* **415**, 327 (2002).

17. C. Lüscher, R. C. Malenka, *Neuron* **69**, 650 (2011).

18. M. S. Brodie, T. V. Dunwiddie, *Naunyn Schmiedebergs Arch Pharmacol* **342**, 660 (1990).

19. R. Chen *et al.*, *Proc Natl Acad Sci USA* **103**, 9333 (2006).

20. B. Pan, C. J. Hillard, Q.-S. Liu, *Journal of Neurosci* **28**, 1385 (2008).

21. Q.-S. Liu, L. Pu, M.-M. Poo, *Nature* **437**, 1027 (2005).

22. M. A. Ungless, J. L. Whistler, R. C. Malenka, A. Bonci, *Nature* **411**, 583 (2001).

23. T. E. Robinson, K. C. Berridge, *Brain Res. Brain Res. Rev.* **18**, 247 (1993).

24. C. Bellone, C. Lüscher, *Nat Neurosci* **9**, 636 (2006).

25. M. T. C. Brown *et al.*, *PLoS ONE* **5**, e15870 (2010).

26. S. Ikemoto, *Brain Res Rev* **56**, 27 (2007).

27. D. Belin, B. J. Everitt, *Neuron* **57**, 432 (2008).

28. V. Pascoli, M. Turiault, C. Lüscher, *Nature* **481**, 71 (2012).

29. J. W. Grimm, B. T. Hope, R. A. Wise, Y. Shaham, *Nature* **412**, 141 (2001).

30. M. Mameli *et al.*, *Nat Neurosci* **12**, 1036 (2009).

31. D. Kätzel, B. V. Zemelman, C. Buetfering, M. Wölfel, G. Miesenböck, *Nat Neurosci* **14**, 100 (2011).

32. S. Zhao *et al.*, *Eur J Neurosci* **19**, 1133 (2004).

33. S. Schoch *et al.*, *Nature* **415**, 321 (2002).

34. V. Gradinaru *et al.*, *Cell* **141**, 154 (2010).

35. A. A. Grace, B. S. Bunney, *Neuroscience* **10**, 301 (1983).

Acknowledgments:

We thank Camilla Bellone, Mauro Serafin and the members of the Lüscher laboratory for suggestions on the manuscript. We thank Cyril Creton for support with the stereotaxic injections and Matthew Brown for support in the *in vivo* electrophysiology experiments. We also thank Gero Miesenböck for generously providing the GADCre mice and Susanne Schoch for generously providing the Rim1$\alpha^{-/-}$ mice. This work is supported by the Swiss National Science Foundation (C.L.) and ‘‘Synapsy’’, a National Competence Center in Research (NCCR) of the Swiss Confederation on the synaptic basis of mental disorders. C.B. performed *in vitro* electrophysiological experiments and analyzed the data. C.B. and V.P performed retrograde tracer experiments and behavior experiments. J.W., K.R.T. and C.Y. performed *in vivo* electrophysiology experiments and analyzed the data. J.W. performed immunohistochemistry. D.H. performed *in vitro* electrophysiological experiments. M.R. analyzed the data. C.L. designed the study. C.L. and C.B. wrote the manuscript with the help of D.H., K.R.T. and V.P.

Figure 1:

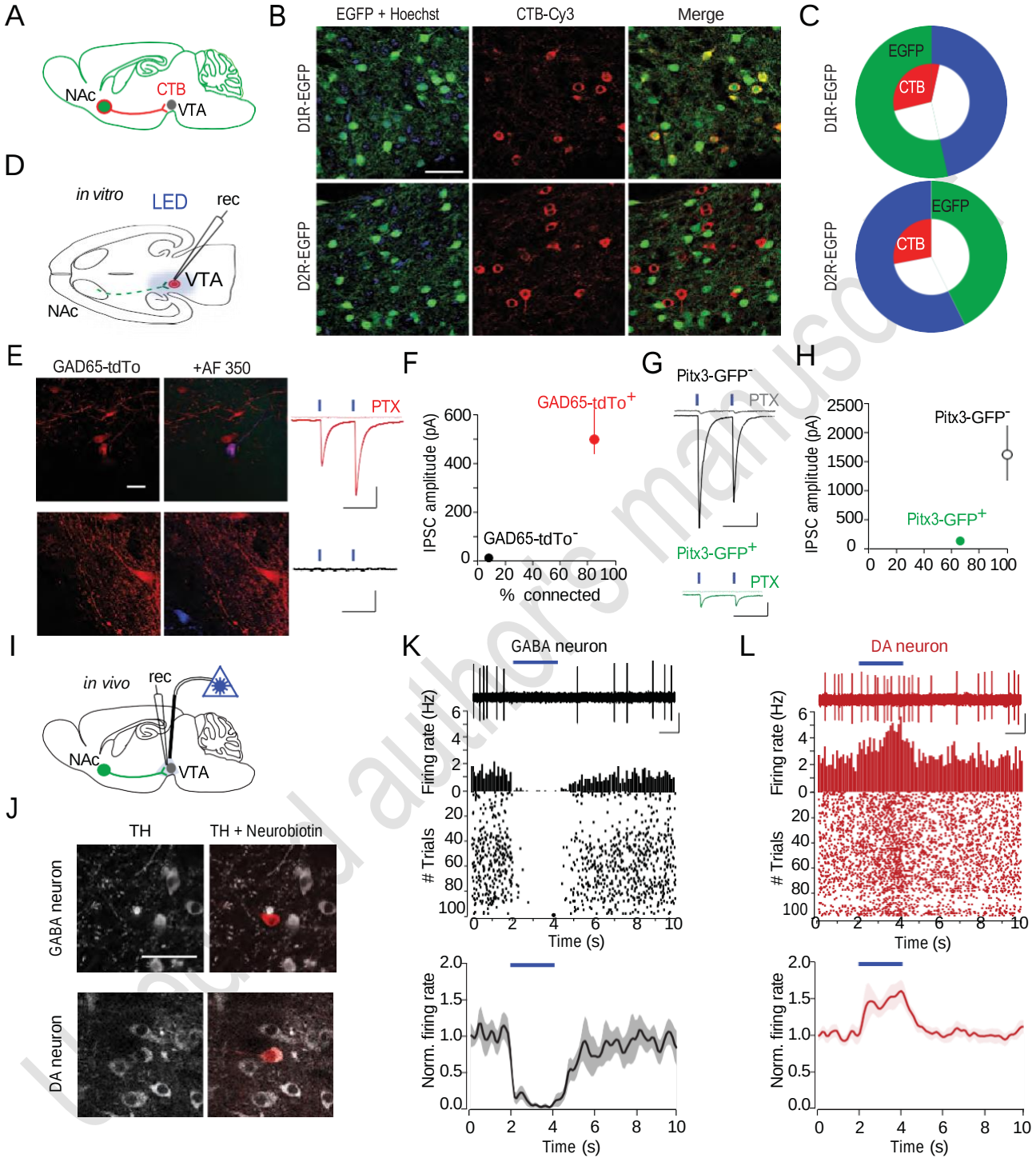

Fig.1. VTA projecting MSNs express D1Rs and disinhibit VTA DA neurons *in vivo* by preferentially targeting VTA GABA neurons (A) Experimental setup: CTB-Cy3 injected into VTA retrogradely labeled NAc MSNs projecting to the VTA. BAC transgenic mice, expressing EGFP in D1R- or D2R-MSNs were used for characterization. (B) Representative confocal immunofluorescence images of NAc slices from D1R- or D2R-EGFP positive mice (green) injected intra-VTA with CTB-Cy3 (red). Nuclear stain Hoechst in blue. Scale bars: 50 μm.

(C) Concentric pie charts representing the percentages of EGFP-positive (green) neurons and CTB-Cy3 labeled cells (red) as proportion of total cell number (blue) in each mouse line. Overlap between the outer and inner segments represents co-localization. (D) Experimental setup: ChR2 was expressed in the NAc of GAD65Cre or Pitx3-GFP mice. VTA-projecting MSN terminals were stimulated with blue LED light in acute slices that contained the VTA. (E) Representative fluorescent images of VTA slices from GAD65Cre mice showing a tdTomato-positive neuron (top) (GAD65-tdTo, red) or GAD65-tdTo-negative neuron (bottom) filled with Alexa fluor ®350 hydrazide (AF 350, blue). Scale bar: 20um. Right: whole-cell voltage-clamp recordings of the same cells as on the left showing presence (top) or absence (bottom) of light-evoked IPSCs. Scale bars: 50 ms, 100 pA. (F) Graph showing average amplitude of IPSCs recorded in GAD65-tdTo-positive and -negative neurons as a function of the percentage of connected neurons. Data are mean ± s.e.m. (G) Representative traces of whole-cell voltage-clamp recordings of Pitx3-GFP-positive and -negative neurons, respectively, showing presence of light-evoked IPSCs. Scale bars: 50 ms, 200 pA. (H) Average amplitude of light-activated IPSCs plotted against the proportion of connected cells in Pitx3-GFP-positive and -negative cells. Data are mean ± s.e.m. (I) Schematic of experimental setup: *In vivo* single-unit recordings of VTA neurons were performed while ChR2-Venus expressing MSN afferents were optogenetically stimulated through a guide cannula targeting the VTA. (J) Immunofluorescence images of the VTA of *in vivo* juxtacellularly labeled neurons with neurobiotin (red) and tyrosine hydroxylase (TH) staining (white). Examples of a labeled DA neuron co-localizing with TH (bottom) and a putative GABA neuron, not co-localizing (top) with TH. Scale bar: 50 μm. (K-L) Top: *In vivo* single unit recordings of the same cells as in (J). Representative traces, peristimulus time histograms and raster plots of GABA neurons (K) and DA neurons (L). Blue bar: 2 s laser pulse. Scale bars: 1 s, 1 mV. Bottom: plots of the average firing rates during blue laser stimulation of GABA neurons (K) and DA neurons (L) identified with juxtacellular labeling. Data are mean ± s.e.m.

Figure 2:

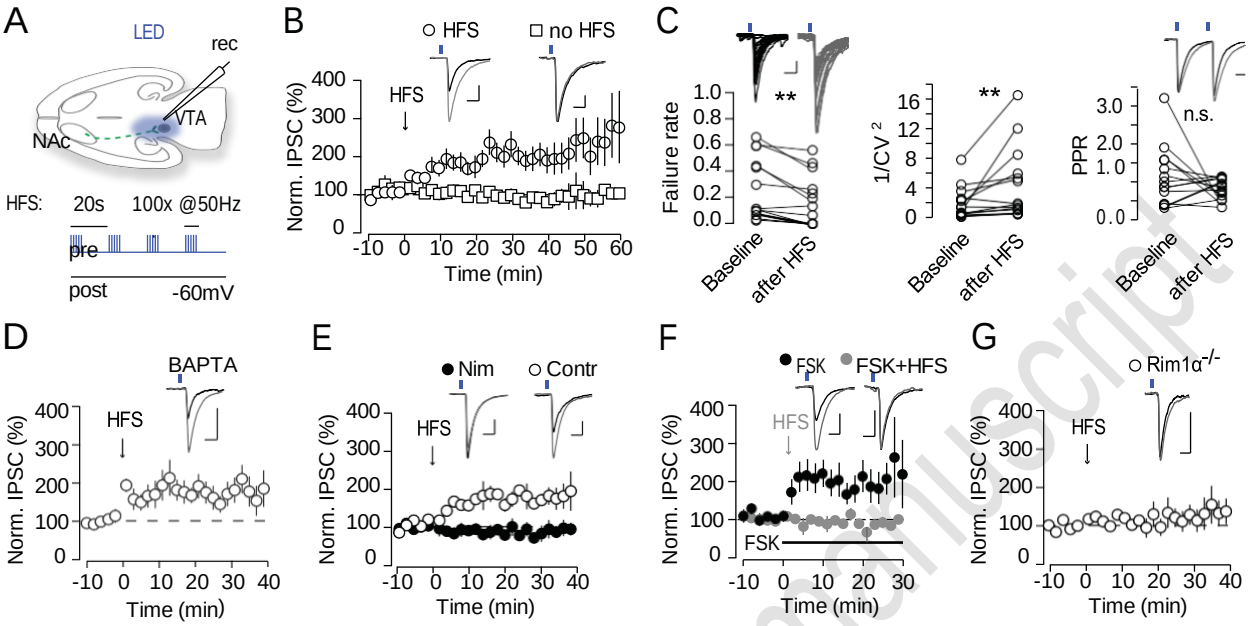

Fig. 2. HFS induces cAMP-PKA-dependent plasticity at synapses between NAc MSNs and their target neurons in the VTA (A) Experimental setup: *in vitro* whole-cell recordings of VTA neurons in horizontal acute slices from wt mice. Plasticity induction protocol: MSN terminals were stimulated by four trains of 100 light pulses at 50 Hz, each 20 s apart (HFS) while the postsynaptic cell was kept in voltage-clamp at -60 mV. (B) HFS of MSN terminals potentiates IPSC amplitudes. Squares indicate time course of IPSCs in the absence of HFS. Example traces of IPSCs at baseline (black) and after HFS (grey). All scale bars: 100 pA, 10 ms. (C) Plots representing group data for failure rate, coefficient of variation ($1/CV^2$) and paired pulse ratio (PPR) at baseline and after HFS. (D) Intracellular loading of BAPTA did not block HFS-induced increase in IPSC amplitude. (E) Continuous bath- application of nimodipine (Nim) blocked HFS-induced potentiation. (F) Bath-application of FSK (black bar) induced potentiation of IPSC amplitudes (black circles) while it occluded HFS-induced potentiation of IPSCs (grey circles). (G) HFS failed to induce potentiation in Rim1$\alpha^{-/-}$ mice. Data are mean ± s.e.m.

Figure 3:

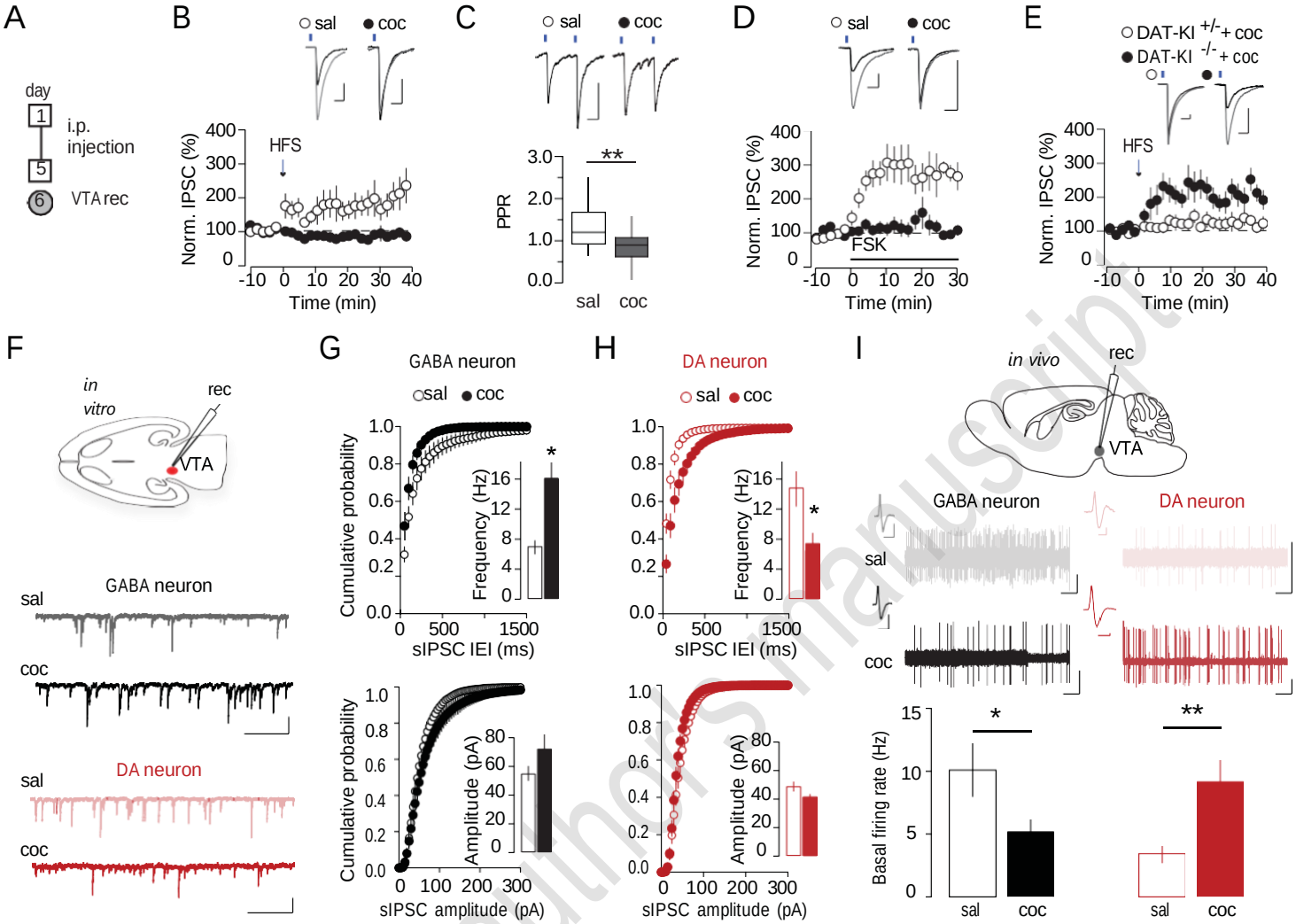

Fig. 3. *In vivo* cocaine treatment induces potentiation at synapses between NAc MSNs and VTA GABA cells and disinhibits VTA DA neurons (A) Protocol of *in vivo* cocaine treatment. (B) HFS failed to induce potentiation in cocaine-treated mice as compared to saline-treated animals. Scale bars 100 pA, 10 ms. (C) PPR example traces and boxplots showing group data of light-evoked IPSCs recorded in VTA GABA cells in saline- and cocaine-treated mice. Scale bars: 20 ms, 50 pA. (D) Bath-application of FSK failed to induce potentiation of IPSC amplitude in cocaine-treated mice as compared to saline-treated mice. Scale bars: 100 pA, 10 ms. (E) HFS successfully induced potentiation in homozygous DAT_{KI} mice chronically treated with cocaine while potentiation could not be fully induced in heterozygous DAT_{KI} mice. Scale bars: 100 pA, 10 ms. (F) Experimental setup and representative example traces of sIPSCs recorded in acute VTA slices in fluorescence-identified GABA (black) and DA (red) neurons. Scale bars: 50 pA, 0.5 s. (G-H) Histograms representing the cumulative probability distribution of sIPSC inter-event intervals (IEI) and amplitudes in VTA GABA neurons (G) and DA neurons (H) from mice chronically treated with saline and cocaine, respectively. Insets: sIPSC frequencies and amplitudes plotted as bar graphs for saline and cocaine treatment. (I) Experimental setup and representative example traces of *in vivo* recordings of VTA GABA and DA neurons, identified by their action potential width (insets, scale bars GABA: 2 ms, 10 mV, DA: 2 ms, 20 mV). Scale bars: 1s, 10 mV. Bottom: bar graph representing group data for firing rates of VTA DA and GABA neurons in saline- and cocaine-treated animals. Data are mean ± s.e.m.

Figure 4:

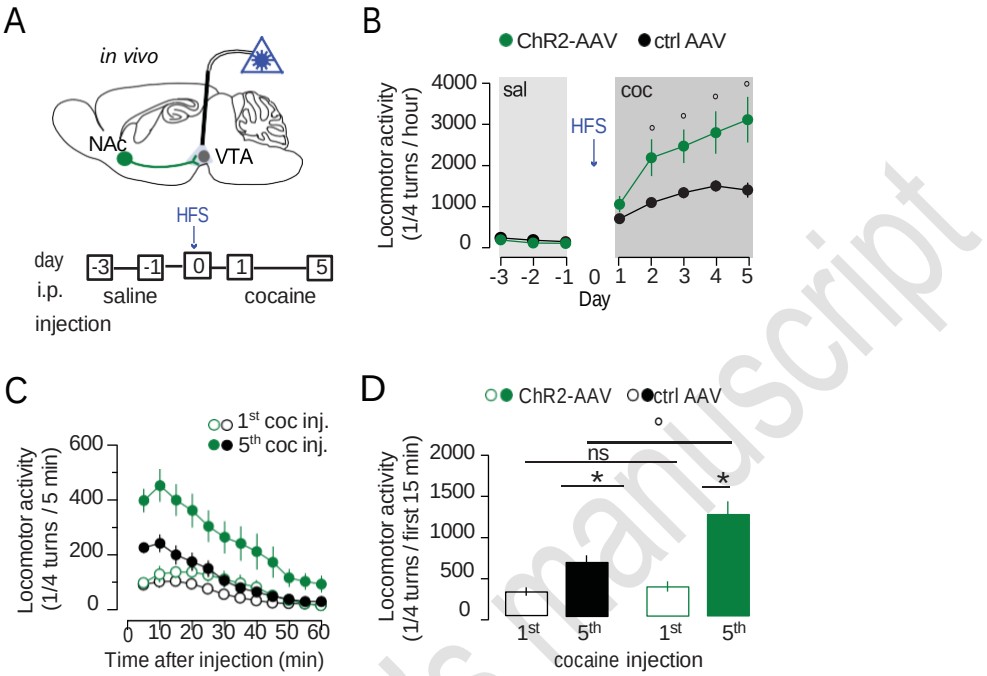

Fig. 4. Disinhibitory synaptic plasticity between D1R-MSNs and VTA GABA neuron enhances cocaine-induced locomotor sensitization (A) Experimental setup and injection protocol. (B) Locomotor activity represented by ¼ turns done in the circular corridor in 1 hour immediately after saline (days -3 to -1) or cocaine (days 1 to 5) injections (i.p.). Cocaine-induced sensitization of the locomotor activity is enhanced by application of the HFS in animals infected with ChR2 AAV compared to animals infected with a control AAV. (C) Locomotor activity as function of time (during 1 hour following injection) recorded on day 1 after the first cocaine injection (acute) and on day 5 (last injection). (D) Individual values and bar graphs representing the locomotor activity recorded during the first 15 min after cocaine injection on days 1 and 5 showing larger senstization in the ChR2-AAV group. Data are mean ± s.e.m.

Supplementary Materials:

Materials and Methods

Subjects: All animal experiments were carried out in accordance with the institutional Animal Care and Use Committee of the University of Geneva and with permission of the cantonal authorities. Experiments were performed on C57BL/6 mice, Gad65Cre mice (*31*), Pitx3-GFP mice (*32*), BAC transgenic drd1a-eGFP mice, BAC transgenic drd2-eGFP mice, DAT-knockin mice (*19*) and Rim1$\alpha^{-/-}$mice (*33*).

Stereotaxic injection: For optogenetic electrophysiology experiments, AAV2/1-CAG-ChR2-Venus (Addgene Plasmid 20071) produced at the University of North Carolina (UNC Vector Core) was bilaterally injected in the NAc of 7-10g C57/BL6 mice, Gad65Cre mice or DATKI mice. AAV-EF1a-DIO-eNpHR 3.0-EYFP (*34*) (UPenn Vector Core) was injected in the VTA of Gad65Cre mice. Pitx3-GFP mice were injected with AAV2/1-CAG-hChR2(H134R)-mCherry (UPenn Vector Core). For labeling of VTA GABA neurons, AAV1-DIO-tdTomato (0.5 µl) produced at University of Pennsylvania (UPenn Vector Core) was additionally injected in the VTA of 7-10g Gad65Cre mice. For the retrograde labeling of VTA projecting NAc MSNs, Cy3-cholera toxin subunit B (1 µl, 1 mg/ml, Invitrogen) in sterile PBS was injected into the VTA of 15g drd1a-eGFP mice and drd2-eGFP mice, respectively. Anesthesia was induced and maintained with isoflurane (Baxter AG, Vienna, Austria) at 5% and 2%, respectively. Mice were placed in a stereotaxic frame (Angle One; Leica, Germany) and craniotomies were performed using stereotaxic coordinates for NAc: ML ± 0.6, AP 1.6, DV -4.2 to -4.75 from bregma and VTA: ML ± 0.9, AP -3.3, DV -4.4 from bregma. Injections were carried out using graduated pipettes (Drummond Scientific Company, Broomall, PA) broken back to a tip diameter of 10-15 µm, at a rate of ~ 0.05 µl*min^{-1} for a total volume of 0.5 µl. Incubation time for all virus experiments was at least 2 weeks, for the CTB experiments 7 days before any other procedures were carried out.

***In vivo* electrophysiology:** Mice were anesthetized with choral hydrate 4% (480 mg/kg i.p.) and maintained with supplemental doses as required (120 mg/kg i.p.). Mice were positioned in a stereotaxic frame (Angle One) and their body temperature was maintained at 36-37°C using a homeothermic heating pad (Harvard Apparatus). Anesthesia was continually monitored by testing reflexes to gentle corneal stimulation and a cutaneous pinch. A craniotomy was performed to expose the cortex overlying the left VTA. Recording electrodes were pulled with a vertical puller (Narishige, Tokyo, Japan) from borosilicate glass capillaries (Harvard Apparatus). Electrodes were broken back to give a final tip diameter of 1–2 μm, were filled with a saline solution (0.5M NaCl) and lowered into the VTA at a 10° angle (coordinates from bregma: AP -3.0- -3.4, ML -1.1- -1.4, DV -3.9- 4.5). A reference electrode was placed in the subcutaneous tissue. Electrical signals were AC coupled, amplified (Neurodata IR 183; Neurodata Instruments Corp.), and monitored in real time using an audiomonitor (custom made). Any 50 Hz noise was eliminated using a Humbug (Quest Scientific, Vancouver, Canada). Signals were digitized at 20 kHz (for waveform analysis) or 5 kHz and stored on hard disk using a custom-made program within IGOR (WaveMetrics). The bandpass filter was set between 0.3 and 5 kHz. Cell types were distinguished based on established electrophysiological properties (DA neurons: biphasic action potential of more than 1.1 ms duration) (*35*).

Simultaneous light stimulation: A craniotomy was performed to expose the cortex overlying the left VTA, of a size large enough to accommodate the guide cannula (Plastics One) and the recording electrode. The cannula was stereotaxically positioned and slowly lowered vertically into position at the dorsal boundary of the VTA (coordinates from bregma: AP -3.3, ML -1.3, DV -4.4, 10° angle). Dental cement (Lang Dental) was used to secure the cannula whilst taking care not to allow cement to cover the craniotomy. A fiber optic cable (Thorlabs) was then lowered through the guide cannula so that ~50 μm of fiber protruded from the guide cannula, and attached to a 473 nm solid-state laser (Crystalaser, Reno, NV) for optical excitation or an amber laser (593 nm, Shangai Dream Laser Technology Co., Ltd) for optical inhibition. The laser was controlled using the Igor program via a TTL box. After baseline recording of the spontaneous activity of VTA cells, the laser was switched on for 2 s continuously and off for 8. This optical stimulation was repeated 100 times for blue light stimulation of ChR2 and 30 times for amber light stimulation of halorhodopsin. The processed data were displayed as event raster plots,

binned peristimulus time histograms (PSTHs), or firing rate plots. Event raster plots show the time markers of detected activity of 100 consecutive light responses. For the PSTHs, bins of 100 ms width were analyzed. Baseline firing rate values were obtained by calculating the mean and standard error of counts per bin of the initial 1.5 s of the recording. Light stimulation firing rate values were obtained by calculating mean and standard error of counts per bin of 1.5 s, 500 ms after light onset. Firing rates during light stimulation were normalized by dividing all values of the 1.5 s interval by the 1.5 s at baseline. Data for firing rates are plotted as mean and s.e.m.

Juxtacellular labeling: Recording electrodes for electrophysiological experiments were filled with a 0.5M NaCl solution containing 1.5% neurobiotin (Vector Laboratories). Following electrophysiological recordings, neurons were juxtacellularly labeled with neurobiotin for confirmation of cell type and position (Pinault, 1996). Briefly, positive current pulses were applied through the recording electrode to the neuron. Current amplitude was increased until neuronal action potentials became entrained with the current pulses. This was continued for 30 s – 10 min, at which point the current was switched off and the electrode reversed away slowly from the neuron. After allowing 30 min - 4 hours for transport of the neurobiotin within the neuron, animals were prepared for immunohistochemical processing.

Immunohistochemistry: Animals were given a lethal dose of choral hydrate and perfused transcardially with 4 % paraformaldehyde (PFA) in phosphate buffer (PBS). Brains were removed and left in 4% PFA overnight before being transferred into PBS ready for immunohistochemical processing. Brains were washed in PBS and 50 μm horizontal sections of the VTA were prepared. Slices were immersed in PBS containing 0.3% triton for tissue permeabilization. To reveal labeled cells using the juxtacellular method, slices were incubated at 4°C for 2-4 h in Streptavidin-Cy3 (1:1000, Invitrogen). Following retrieval of the labeled cell body, selected tissue sections were incubated (4° C, 2 nights) in PBS containing primary antibodies against tyrosine hydroxylase (TH, mouse anti-TH; 1:1000, Sigma). For visualization of TH immunoreactivity fluorescent conjugates were used (AlexaFluor 647-conjugated Donkey anti-mouse; 1:500, 4°C, 4h; Invitrogen). Sections were then mounted in moviol for viewing with a confocal laser- scanning microscope (Zeiss LSM 510META). For the CTB experiment, brains were fixed *in situ* twelve days after injection by intracardiac perfusion of 4 % PFA in 0.1 M

Na_2HPO_4-NaH_2PO_4 buffer, pH 7.5, delivered with a peristaltic pump at 20 ml/min for 5 min. Brains were removed and post-fixed overnight in the same fixative solution. Coronal NAc sections (30 µm) were cut with a vibratome (Leica) and then kept in a solution containing 30 % ethylene glycol, 30 % glycerol, 0.1 M phosphate buffer, and 0.1 % diethylpyrocarbonate (DEPC; Sigma Aldrich) at -20°C until they were processed for immunohistochemistry. Free-floating sections were rinsed in Tris-buffered saline (TBS; 0.25 M Tris and 0.5 M NaCl, pH 7.5 containing NaF 0.1 M) and incubated for 15 min in 0.2 % Triton X- 100 in TBS. After rinses, sections were saturated for 1 h with 3 % BSA, 0.2 % Triton in TBS. Sections were then rinsed in TBS and incubated overnight at 4°C with primary antibody (anti-GFP, 1/300, Invitrogen). After rinses, sections were incubated for 2 h at RT with the following secondary antibody: FITC-conjugated anti-rabbit (1/100, Jackson Lab.). Nuclei were then counterstained with Hoechst (Invitrogen) and sections mounted under coverslips with moviol. Pictures of the nucleus accumbens were taken using laser-scanning microscope (Zeiss LSM 510META) with a 40 x oil immersion objective.

Electrophysiology in acute brain slices: Horizontal slices of the midbrain were prepared using a vibratome (Leica Instruments) in ice cold artificial cerebrospinal fluid (ACSF) containing: NaCl 119 mM, KCl 2.5 mM, $MgCl_2$ 1.3 mM, NaH_2PO_4 1.0 mM, $NaHCO_3$ 26.2 mM, $CaCl_2$ 2.5 mM and glucose 11 mM, continuously bubbled with 95 % O_2 and 5 % CO_2. Slices were submerged in 34°C ACSF for 30 min and allowed to recover for another 30 min at room temperature. They were subsequently transferred to the recording chamber, superfused with 2.5 ml min^{-1} ACSF at nearly physiological temperature (30-32°C). Slices were visualized on an Olympus BX45 scope equipped with a 40x objective lens. Neurons were recorded by means of whole-cell voltage-clamp at -60 mV. Borosilicate glass pipettes (Harvard apparatus LTD) were prepared at a resistance range of 2-4 MΩ. The internal solution contained: KCl 100 mM, potassium gluconate 30 mM, $MgCl_2$ 4 mM, sodium creatine phosphate 10 mM, Na_2ATP 3.4 mM, Na_3GTP 0.1 mM, EGTA 1.1 mM and HEPES 5 mM. For sIPSC recordings, the internal solution contained: 130 mM CsCl, 4 mM NaCl, 2 mM $MgCl_2$, 1.1 mM EGTA, 5 mM HEPES buffer, 2 mM Na_2ATP, 5 mM sodium creatine-phosphate, 0.6 mM Na_3GTP and 0.1 mM spermine. The calculated reversal potential in both internal solutions for Cl^- was -4.9 mV. Currents were amplified, filtered at 2 kHz (Multiclamp 200B, Axon Instruments) and digitized at

10 kHz (National Instruments PCI-MIO-16E-4 card) and saved on a hard disk (IgorPro v.6.0, WaveMetrics Inc.). The liquid junction potential was small (-4 mV) and traces were therefore not corrected. Access resistances were monitored by a hyperpolarizing step of -4 mV at the onset of every sweep and the experiment was discarded if the access resistance changed by more than 20 %. I_h currents were activated by a 500 ms hyperpolarizing step from -60 mV holding potential to -120 mV. ChR2 was stimulated by flashing 470 nm blue light (0.1–2 ms) at 0.1 Hz through the light path of the microscope using an LED (Thorlabs) powered by an LED driver (Thorlabs, LEDD1A) under computer control. Light-evoked IPSCs were recorded in the presence of kynurenic acid (2 mM). Paired pulse ratios were evoked at an interval of 50 ms. Representative example traces are shown as average of 30 consecutive IPSCs. For the plasticity experiments, representative traces were taken from the last 5 min of the baseline and at least 20 min after the induction of the plasticity.

Electrophysiology data analysis: Electrophysiological data were analyzed in IGOR, Prism and Mini Analysis software (Synaptosoft). *In vivo* firing rates were statistically analysed using student's t-test for unpaired data. Light-evoked changes of firing rates in DA neurons were compared using student's t-test for paired data. sIPSC distributions were statistically analyzed using the nonparametric two-sample Kolmogorov-Smirnov test (KyPlot) and student's t-test for unpaired data. HFS effect on light-evoked IPSC amplitudes, failure rates, $1/CV^2$ and PPRs was evaluated using Wilcoxon signed rank test or student's t-test for paired data.

Drug treatment: C57/BL6 mice or DAT_{KI} mice were injected intraperitoneally (i.p.) with cocaine (15 mg/kg) or 0.9 % saline with a 26G hypodermic needle to minimize stress.

Locomotor sensitization: BL6/C57 mice were cannulated in the VTA (see above) and allowed at least 1 week of recovery before any behavioral experiments were carried out. Locomotor activity was measured as the number of quarter turns completed by a mouse in a circular corridor. The locomotor apparatus was placed under a video tracking system (Any-maze, Stoelting) and measurements were made automatically by the software. After 3 days of habituation to the test apparatus, mice underwent the experimental procedure, which consisted of one session of in *vivo* HFS through a fiber optics and connected solid state laser (Crystalaser,

Reno, NV) 24h later and 5 daily injections of 15mg/kg cocaine i.p. starting 24h after HFS. After mice received cocaine, they were immediately placed in the circular corridor for 60 min. For statistical analysis of the day effect, the ChR2 effect and the interaction, two way ANOVA for repeated measures and Bonferroni Post-hoc analysis for within-group analysis was used.

Supplementary Figure S1:

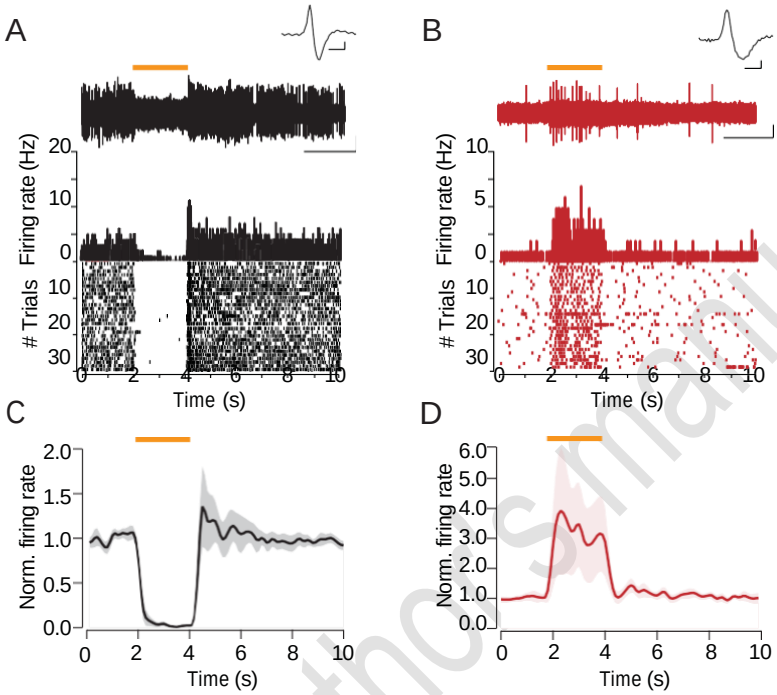

Supplementary Fig. S1. Optogenetic inhibition of VTA GABA neurons with halorhodopsine disinhibits VTA DA neurons *in vivo* (A-B) *In vivo* single unit recordings of VTA neurons, identified by action potential width (insets, scale bars: 1 ms, 2 mV). Representative traces (top), peristimulus time histograms (middle) and raster plots (bottom). Scale bars: 2 s, 5 mV. (A) Example of a putative GABA neuron. A 2 s amber laser pulse (orange bar) decreases the firing rate. (B) Example of a putative DA neuron. A 2 s amber laser pulse (orange bar) increases the firing rate. (C-D) Plots of the normalized firing rates during amber laser stimulation of VTA neurons. Data are mean ± s.e.m. (C) Firing rate of GABA neurons was decreased by 97.4 ± 1.3 % during light stimulation (n = 4). (D) Firing rate of DA neurons was increased by 314.8 ± 132.6 % during light stimulation (n = 9).

Supplementary Figure S2:

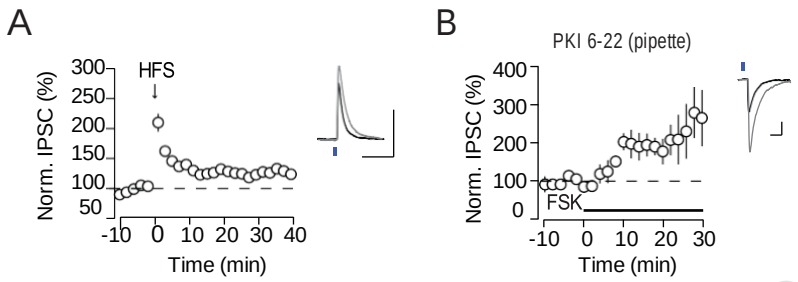

Supplementary Fig. S2. Presynaptic potentiation is induced in outward IPSCs

(A) HFS induces synaptic potentiation in GABA neurons patched with low chloride internal solution (135 ± 8% of baseline, n = 8). Scale bar: 40 pA, 10 ms. (B) FSK (black bar) potentiates IPSCs in the presence of the PKA blocker PKI (20 μM) in the postsynaptic cell (178 ± 27 % of baseline, n = 5). Scale bars: 40 pA, 10 ms. Data are mean ± s.e.m.

Supplementary Figure S3:

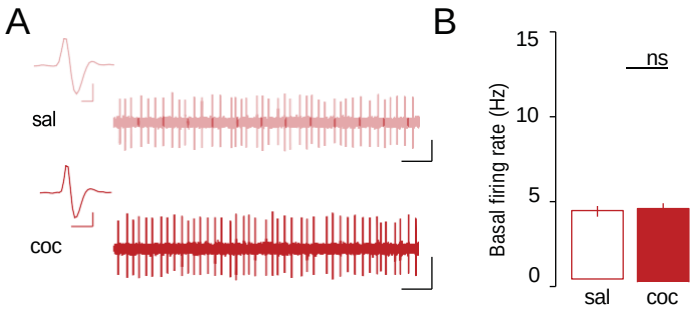

Supplementary Fig. S3. One single cocaine injection does not affect DA neuron firing rates 24h after injection. (A) Representative example traces of *in vivo* recordings of VTA DA neurons 24 h after one single injection of saline or cocaine (15 mg/kg i.p.). DA neurons were identified by their action potential width (insets, scale bars: 1 ms, 2 mV). Scale bars: 1 s, 4 mV. (B) Bar graph representing group data for firing rates of VTA DA after one single saline or cocaine injection (saline: 4.1 ± 0.2 Hz, n = 112; cocaine: 4.3 ± 0.2 Hz, n = 76, $p > 0.05$).